Check for updates

Seasonal and short-term variations in atmospheric potential oxygen at Ny-Ålesund, Svalbard

By DAISUKE GOTO[1*], SHINJI MORIMOTO[2], SHUJI AOKI[2], PRABIR K. PATRA[3] and TAKAKIYO NAKAZAWA[2],   [1]*National Institute of Polar Research, Research Organization of Information and Systems/SOKENDAI (The Graduate University for Advanced Studies), Tachikawa, Japan;* [2]*Center for Atmospheric and Oceanic Studies, Graduate School of Science, Tohoku University, Sendai, Japan;* [3]*Department of Environmental Geochemical Cycle Research, Japan Agency for Marine-Earth Science and Technology (JAMSTEC), Yokohama, Japan*

ABSTRACT

Oxygen in the atmosphere undergoes variations and changes in response to biospheric activities, ocean–atmosphere exchange and fossil fuel combustion. Continuous *in situ* measurements of atmospheric $\delta(O_2/N_2)$ and CO_2 mole fraction were started at Ny-Ålesund, Svalbard (78.93°N, 11.83°E, 40 m a.s.l.) in November 2012. Atmospheric potential oxygen (APO) calculated from the measured O_2 and CO_2 values during November 2012–January 2015 show a clear seasonal cycle with a peak-to-peak amplitude of approximately 50 per meg. The seasonal cycle of APO simulated using an atmospheric transport model, with prescribed oceanic O_2, N_2 and CO_2 fluxes at monthly time intervals, is in excellent agreement with the observed APO. However, in spring and early summer, high values of APO are observed irregularly on a timescale of hours to days. By comparing backward trajectories of air parcels released from the site with distributions of marine net primary production (NPP), and tagged tracer experiments made using the atmospheric transport model for APO, it is found that these high APO fluctuations are primarily attributable to O_2 emissions from the Greenland Sea, the Norwegian Sea and the Barents Sea, due to marine biological productivity. Marine net community production, estimated based on the sea-to-air O_2 flux derived from observed APO fluctuations, agrees with NPP obtained from satellite observations within an order of magnitude. The results obtained in this study have still some uncertainties, but our continuous observations of atmospheric $\delta(O_2/N_2)$ and CO_2 mole fraction at Ny-Ålesund can play an important role in detecting possible changes in the carbon cycle in the near future.

Keywords: atmospheric potential oxygen (APO), net community production, atmospheric transport model, air–sea O_2 exchange, Ny-Ålesund

1. Introduction

Understanding the sources and sinks of O_2 and CO_2 is important for advancing our knowledge of the global carbon cycle. Atmospheric O_2 and CO_2 are closely related to each other through terrestrial biospheric photosynthesis and respiration, as well as the combustion of fossil fuel. However, the two gases are exchanged independently between the atmosphere and the ocean. Global oceanic and terrestrial biospheric carbon sinks can therefore be estimated separately by analysing long-term changes in atmospheric O_2 and CO_2 (e.g. Keeling and Shertz, 1992; Keeling and Manning, 2014).

Variations in atmospheric O_2 are usually expressed as a change in the ratio of O_2 to N_2, as follows (Keeling and Shertz, 1992):

$$\delta(O_2/N_2) = \left[\frac{(O_2/N_2)_{sample}}{(O_2/N_2)_{reference}} - 1 \right] \times 10^6 \tag{1}$$

where $(O_2/N_2)_{sample}$ and $(O_2/N_2)_{reference}$ refer to the mole ratios of O_2/N_2 in the sample air and reference air, respectively. The value of $\delta(O_2/N_2)$ defined by Equation (1) is commonly reported in the unit of 'per meg'. Change of 4.8 per meg in $\delta(O_2/N_2)$ corresponds to 1 μmol mol^{-1} change in O_2, when O_2 and CO_2 vary in the atmosphere at the $-O_2$:CO_2 exchange ratio of 1.0. To eliminate the influence of terrestrial biospheric activity on $\delta(O_2/N_2)$, Stephens et al. (1998) defined atmospheric potential oxygen (APO) in per meg unit as follows:

$$APO = \delta(O_2/N_2) + \frac{\alpha_B}{X_{O_2}} \times (CO_2 - 355) \tag{2}$$

where α_B is 1.1 (Keeling and Manning, 2014), which is the $-O_2$:CO_2 exchange ratio for terrestrial biospheric activity, X_{O_2} is the mole fraction of O_2 in the atmosphere, CO_2 is the mole

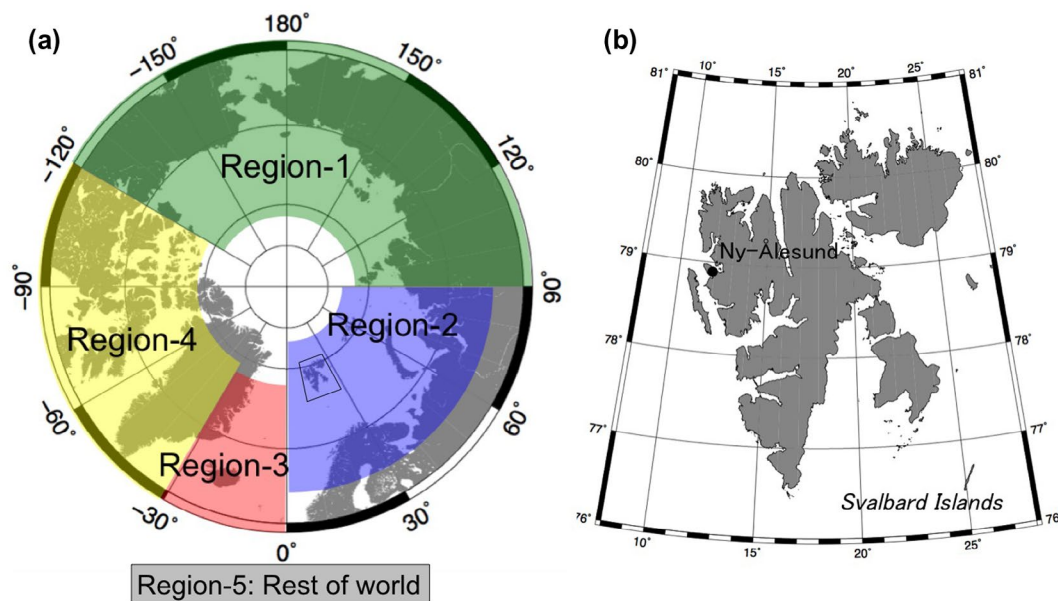*Corresponding author. e-mail: goto.daisuke@nipr.ac.jp

1

Fig. 1. Maps showing (a) the location of Ny-Ålesund (78.93°N, 11.83°E) in Svalbard and the five regions selected for tagged tracer experiments of APO and (b) an enlarged map view of the area indicated by the polygon in the left-hand figure.

fraction of CO_2 in the atmosphere (ppm in mole fraction) and 355 is the CO_2 mole fraction (µmol mol^{-1}) of Tohoku University O_2 primary standard. APO, thus defined, is mainly governed by air–sea O_2 exchange and has previously been used to evaluate air–sea O_2 flux (e.g. Tohjima et al., 2012). Although APO does not exclude the influence of fossil fuel combustion, its contribution is much reduced by defining it as above, since the $-O_2$:CO_2 exchange ratios in burning fossil fuels are not so different from α_B (Keeling and Manning, 2014).

Simultaneous observations of atmospheric $\delta(O_2/N_2)$ and CO_2 mole fraction have been systematically conducted since the early 1990s using discrete flask sampling with subsequent laboratory analysis (e.g. Bender et al., 2005; Manning and Keeling, 2006; Ishidoya et al., 2012a, 2012b; Tohjima et al., 2015). These observations revealed spatio-temporal variations in atmospheric $\delta(O_2/N_2)$ and APO. Measurements of atmospheric $\delta(O_2/N_2)$ and CO_2 mole fraction have also been made using continuous *in situ* monitors (e.g. Lueker et al., 2003; Lueker, 2004; Yamagishi et al., 2008; van der Laan-Luijkx et al., 2010; Goto et al., 2013a; Ishidoya et al., 2013), revealing small and short-term fluctuations in atmospheric $\delta(O_2/N_2)$ and APO, thereby providing new insight into the carbon cycle. Lueker et al. (2003) and Lueker (2004) observed low values of APO at the Trinidad Head coastal site in California (41.05°N, 124.15°E), lasting for several days or weeks. They attributed the uptake of atmospheric O_2 to O_2-poor deep-sea water, which is transported from the deep ocean to the surface by strong coastal upwelling.

In this paper, we present the results of atmospheric $\delta(O_2/N_2)$ and CO_2 observations obtained for the first two years at the first continuous monitoring site of atmospheric $\delta(O_2/N_2)$

at Ny-Ålesund. We discuss seasonal and short-term variations in the observed APO, and compare these variations with those simulated using an atmospheric transport model. We also estimate sea-to-air O_2 fluxes and marine net community production (NCP) in marginal sea areas, based on observed short-term variations in APO.

2.   Methods

2.1.   Observation site and measurement system

Ny-Ålesund (78.93°N, 11.83°E, 40 m a.s.l.) is located on the west coast of Spitsbergen Island, Svalbard (Fig. 1), and is a base for international Arctic research. The ground surface is generally rocky, with some covering of moss. The annual mean temperature at the base is −4.5 °C, ranging between −12.0 °C in March and +5.8 °C in July. The prevailing surface winds are south-easterly (Maturilli et al., 2013). The ground is typically covered by snow from October to May.

A continuous measurement system for atmospheric $\delta(O_2/N_2)$ and CO_2 was installed and began operating in the Japanese observatory in November 2012, situated ~2 km west-northwest of the central part of Ny-Ålesund (Goto et al., 2013a).

A detailed description of our measurement system has been presented previously (Goto et al., 2013a, 2013b). The system consists mainly of O_2 and CO_2 analysers, a gas handling system and a data acquisition system. We adopted a differential fuel cell analyser (Oxzilla-II) for O_2 measurements and a non-dispersive infrared analyser (Li-6252) for CO_2 measurements. An aspirated

air-intake was mounted on the roof of the observatory and air samples are continuously fed into the measurement system using a diaphragm pump. To remove water vapor from the air sample, two water traps placed in parallel, equipped with a Stirling cooler, are incorporated into the gas handling system: one is cooled to −80 °C to dehumidify the sample, while the other is heated to 50 °C to dry its inside. The cooling and heating of the respective traps are switched every 6 h. Two standard gases with known values of $\delta(O_2/N_2)$ and CO_2 mole fraction, in 48-L aluminium cylinders, are measured every one hour to calibrate the O_2 and CO_2 analysers. By examining a non-linear response of the CO_2 analyser using several standard gases with different CO_2 mole fractions, we confirmed that its influence on the present measured values is negligibly small, within our measurement reproducibility. The $\delta(O_2/N_2)$ and CO_2 mole fractions of the two standard gases were determined against the Tohoku University O_2 primary standard (Ishidoya et al., 2003) and the CO_2 mole fraction scale prepared gravimetrically by Tohoku University in 2010 (TU-X10), respectively. These calibrations were conducted before and after their use, and confirmed there were no appreciable drifts in the respective mole fractions. The measurement reproducibility was estimated to be ±1.4–1.9 per meg for $\delta(O_2/N_2)$ and ±0.03–0.05 ppm for CO_2, based on analyses repeated 266 times for the same air sample over 24 h.

2.2. Atmospheric transport model

To interpret the APO variations observed at Ny-Ålesund, numerical simulations were performed using the CCSR/NIES/ FRCGC (Center for Climate System Research /National Institute for Environmental Studies/Frontier Research Center for Global Change) Atmospheric General Circulation Model (AGCM)-based Chemistry Transport Model (ACTM) developed in Japan Agency for Marine-Earth Science and Technology (JAMSTEC). The ACTM uses a horizontal resolution of approximately 2.8° × 2.8° (T42 spectral truncation) and 1.125° × 1.125° (T106 spectral truncation), with 32 pressure-sigma vertical layers (Patra et al., 2009, 2014). In the model simulations, ocean fluxes of O_2 and N_2 were taken from the TransCom experimental protocol (Garcia and Keeling, 2001; Blaine, 2005), and CO_2 from Takahashi et al. (2009). Emissions of anthropogenic CO_2 were taken from the Emission Database for Global Atmospheric Research (EDGAR, version 4.2) inventory scaled to Carbon Dioxide Information Analysis Center (CDIAC) global totals. Meteorological data used in the model were adjusted to the Japanese 25-year ReAnalysis data (JRA-25) (Onogi et al., 2007), and the atmospheric transport field of the model was validated by Patra et al. (2009). In addition, tagged tracer experiments were performed using the ACTM at T106 resolution to reveal the contributions of different geographical regions to the observed APO variations. The tag-tracer simulations are mass conserving since no chemical loss or gain is modelled in ACTM. In the experiments, five tag regions were assigned, as shown in Fig. 1.

The model-simulated APO values were derived in accordance with Nevison et al. (2008) as follows:

$$APO = \frac{[O_2]^{OC} - \alpha_F[CO_2]^{FF}}{X_{O_2}} - \frac{[N_2]^{OC}}{X_{N_2}}$$
$$+ \frac{\alpha_B\left([CO_2]^{FF} + [CO_2]^{OC}\right)}{X_{O_2}} \qquad (3)$$

where $[O_2]$, $[N_2]$ and $[CO_2]$ are mole fractions of the respective gases calculated for Ny-Ålesund using the model. The superscripts 'OC' and 'FF' denote oceanic and fossil fuel origins, respectively. X_{O_2} and α_B have the same meaning as in Equation (2), while X_{N_2} is the mole fraction of N_2 in the atmosphere and α_F is the global average $-O_2:CO_2$ exchange ratio for fossil fuel combustion. In this study, we adopted $X_{O_2} = 0.2094$, $X_{N_2} = 0.7809$ (Tohjima et al., 2005, 2008), $\alpha_F = 1.4$ (Keeling and Manning, 2014), and α_B have the same meaning as Equation (2).

3. Results and discussion

3.1. Seasonal cycle

Figure 2 shows hourly mean values of atmospheric $\delta(O_2/N_2)$, CO_2 mole fraction and APO for the period from November 2012 to January 2015. The best-fit curves and long-term trends were obtained by applying a digital filtering technique (Nakazawa et al., 1997) to the daily mean values. In this technique, signals with periods of longer than 24 months are regarded as the long-term trend, and the average seasonal cycle is approximated by the fundamental and its first harmonics. The $\delta(O_2/N_2)$ and CO_2 mole fraction decrease and increase secularly, and vary seasonally in opposite phase to each other. The APO shows not only a secular decrease, but also a seasonal cycle that is almost in phase with that of $\delta(O_2/N_2)$.

The results reported by Ishidoya et al. (2012b) from mass spectrometry analyses of weekly flask air samples at Ny-Ålesund are also presented in Fig. 2, for the period from November 2012 to January 2015. Figure 3 compares the $\delta(O_2/N_2)$ values reported by Ishidoya et al. (2012b) using the flask sampling method ($\delta(O_2/N_2)_{flask}$) with the daily mean values from our continuous measurements ($\delta(O_2/N_2)_{daily}$). Each daily mean value was calculated by averaging the measured values over each 24-h period, including the time when the pertinent flask sample was collected. Although $\delta(O_2/N_2)_{flask}$ is on average slightly lower than $\delta(O_2/N_2)_{daily}$ by 0.27 ± 14.48 per meg, the differences are within analytical precision, allowing a direct comparison of the values obtained from both measurements. The correlation coefficient between $\delta(O_2/N_2)_{flask}$ and $\delta(O_2/N_2)_{daily}$ is 0.95, indicating a strong linear relationship.

Seasonal components derived using the digital filtering technique from the observed and simulated APO values are shown
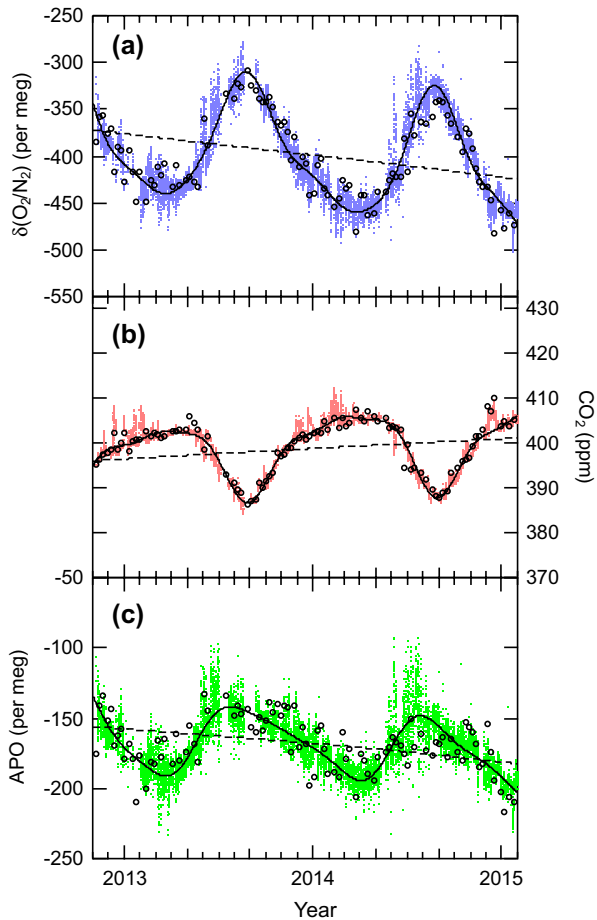
Fig. 2. Temporal variations in (a) $\delta(O_2/N_2)$, (b) CO_2 and (c) APO observed at Ny-Ålesund from November 2012 to January 2015. Dots, solid lines and dashed lines represent hourly mean values, the best-fit curve, and the long-term trend, respectively. The results obtained from discrete flask sampling measurements (Ishidoya et al., 2012b) are shown by open circles. The vertical axis of APO is scaled 1.5 times compared to that of $\delta(O_2/N_2)$.

in Fig. 4. The seasonal cycle of APO obtained from the continuous measurements reaches maximum in July, and minimum in late March, with a peak-to-peak amplitude of approximately 50 per meg. The observed seasonal APO cycle agree fairly well with both resolutions of the ACTM; using the T106 resolution the correlation coefficient is 0.99 (slope of 0.86), and using the T42 resolution the correlation coefficient is 0.98 (slope of 0.80). However, the observed seasonal maximum appears approximately one month earlier than the model simulations. As seen in Fig. 4, the observed APO often shows extremely high values in June and July, probably due to a phytoplankton bloom (Nakaoka et al., 2006). Such high values are not found in the model simulations, since the oceanic O_2, N_2 and CO_2 fluxes are climatological data on a monthly basis.

Ishidoya et al. (2016) reported that the average seasonal cycle of APO obtained by discrete flask sampling at Ny-Ålesund

for the period of 2001–2010 shows significant high values in autumn compared to their simulated APO seasonal cycle. Such a difference in autumn was also found in previous studies (Battle et al., 2006; Tohjima et al., 2012). Ishidoya et al. (2016) attributed cause of this discrepancy to an intrusion of the shallow oxygen maximum layer, which exists in the subsurface ocean in summer, into the surface in autumn when the ocean mixed layer is deepened (e.g. Shulenberger and Reid, 1981). If the oceanic O_2 flux used in the model simulations underestimates this effect, then the calculated APO is lowered. On the other hand, the autumn difference between the observed and simulated seasonal APO cycles is not seen in our results. Considering our short-term observations of 2013–2014, the APO value may have not strongly affected by the oxygen maximum layer in those years. For a better understanding of interannual variations of the seasonal APO cycle, further model studies and longer continuous records of APO are required.

3.2. Short-term fluctuations in APO during spring and summer

The continuous measurements revealed short-term fluctuations in $\delta(O_2/N_2)$, CO_2 and APO in both spring and summer, which were not detected by discrete flask sampling. As an example of such fluctuations, hourly mean values of $\delta(O_2/N_2)$, CO_2 mole fraction and APO measured for May–June 2013 are shown in Fig. 5a and b. It should be noted that the values plotted for each variable in these figures are expressed as deviations from the best-fit curve obtained by applying the digital filtering technique to the measured daily means. The deviations are represented as 'Δ' in the figure. It is seen in Fig. 5a that values of $\delta(O_2/N_2)$ are irregular and high during this period. The CO_2 mole fraction also varies temporally, but inversely with respect to $\delta(O_2/N_2)$. If these fluctuations occur in association with terrestrial biospheric activity, the amplitudes of $\delta(O_2/N_2)$ and CO_2 fluctuations are expected to be nearly equal, since the $-O_2:CO_2$ exchange ratio is 1.1 (Keeling and Manning, 2014). However, the observational results indicate that the CO_2 mole fraction shows much smaller amplitudes than $\delta(O_2/N_2)$, suggesting the exchange ratio is higher than 1.1. For example, the $-O_2:CO_2$ exchange ratio for the $\delta(O_2/N_2)$ and CO_2 variations observed between 30 May and 31 May 2013 is calculated to be 3.96 ± 0.03, showing that the fluctuations are more affected by oceanic process than by terrestrial biospheric process. In this regard, it is well known that the influence of air–sea exchange on atmospheric CO_2 is much smaller due to marine carbonate chemistry (Keeling et al., 1993), compared to O_2. As seen in Fig. 8a to be appeared later, air arrives at Ny-Ålesund on 31 May 2013 after passing over its peripheral seas for 10 days. The CO_2 mole fractions calculated by the ACTM with only air–sea CO_2 fluxes also indicate low values during this period, as seen in Fig. 5a. Engardt et al. (1996) found similar CO_2 dips in spring and early summer
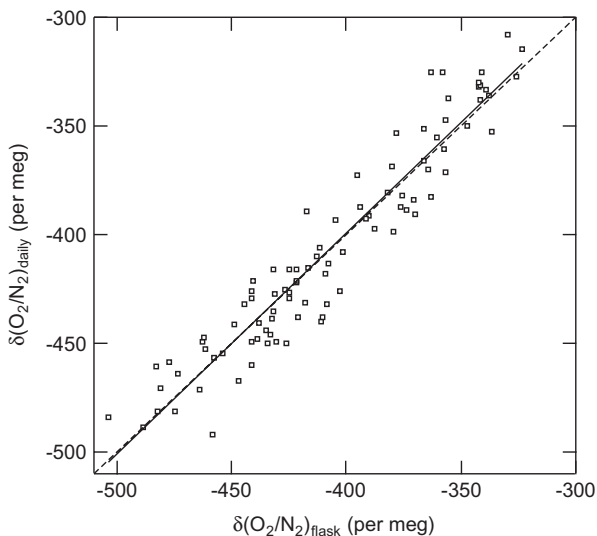
Fig. 3. Comparison of $\delta(O_2/N_2)$ obtained by continuous measurements ($\delta(O_2/N_2)_{daily}$) and discrete flask sampling ($\delta(O_2/N_2)_{flask}$) at Ny-Ålesund. Solid and dashed lines represent a linear regression and one-to-one relationship between $\delta(O_2/N_2)_{daily}$ and $\delta(O_2/N_2)_{flask}$, respectively. $\delta(O_2/N_2)_{daily}$ is the daily mean of continuously measured values for the day when each flask sampling was undertaken.

from continuous measurements at Ny-Ålesund, and suggested that CO_2 uptake in the North Atlantic Ocean and/or by the land biosphere on more southerly latitudes are responsible for such dips. However, it is difficult to separate these causes from only CO_2 variations. Our concurrent observations of $\delta(O_2/N_2)$ and CO_2 would be useful for quantitatively interpreting short-term CO_2 fluctuations, since the $-O_2$:CO_2 exchange

ratio for the ocean process is different from that for the terrestrial biosphere process.

To determine the origin of short-term APO variations observed at Ny-Ålesund, as well as to examine the relationship between air mass transport and APO variation, 10-day backward trajectories from the site were predicted using the CGER/METEX trajectory model (Zeng et al., 2003). In this analysis, air parcels were released from the lowest level of the model (150 m above sea level) every 6 h during the observation period of 9 May–29 June 2013. We confirmed that raising the releasing level by several hundred metres does not appreciably change the results. The predicted trajectories are presented in Fig. 6. Red and blue lines show the trajectories for the respective times when high and low values of APO were observed. Here, we define 'high APO' as the time when ΔAPO exceeds 10 per meg (grey shading in Fig. 5), and all other times as 'low APO'. Figure 6 shows that the APO value varies with the transport path of air. In general, high APO values are observed when air masses arrive at Ny-Ålesund after passing over the seas on the south side of the Svalbard Islands, while most of low or stable APO values are observed when the air arrives from the ice-covered Arctic Ocean.

The APO values simulated using the ACTM are shown in Fig. 5b. Although the seasonal APO cycles for the two model resolutions (T42 and T106) are in fairly good agreement with each other, the observed short-term APO variations agree much better with the simulated APO values of T106 (correlation coefficient = 0.52, slope = 0.41) than those of T42 (correlation coefficient = 0.32, slope = 0.28). This indicates that higher resolution transport models would be better for interpreting short-term APO variations. However, much finer model resolutions
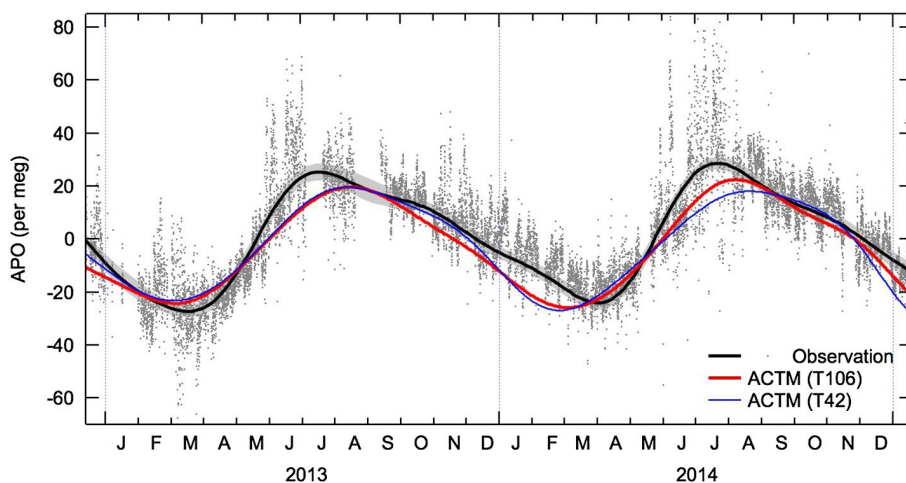

Fig. 4. Seasonal components of APO obtained from continuous measurements (grey dots) for the period of 2013–2014 at Ny-Ålesund, detrended using the digital filtering technique. Black solid line is the best-fit curve of the observed seasonal APO components. Error band (grey shade) represents the uncertainty of the best-fit curve of seasonal APO components estimated by a bootstrap analysis (Press et al., 2007). The results of model simulations with two different resolutions (T42 and T106) for the same period with continuous measurements are shown by red and blue solid lines, respectively.
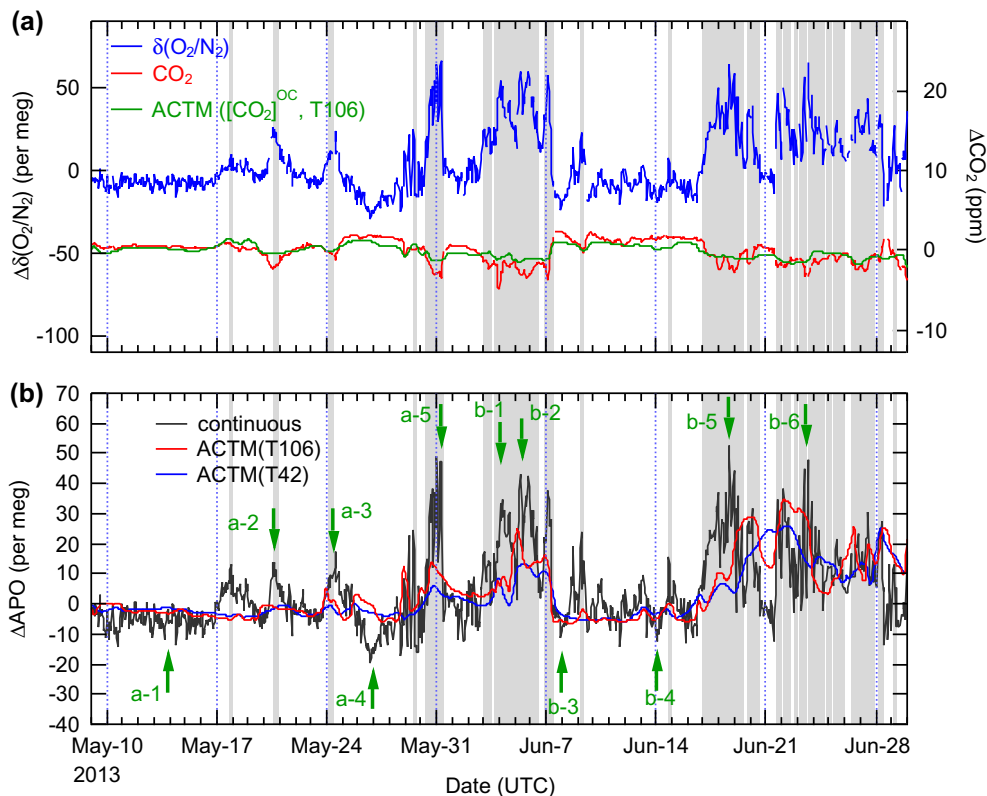
Fig. 5. Temporal variations in (a) $\delta(O_2/N_2)$ and CO_2 and (b) APO observed at Ny-Ålesund for the period from 9 May to 29 June 2013. Green arrows marked a-1–a-5 and b-1–b-6 represent the times when air parcels were released for the backward trajectory calculations (see Fig. 8). The model-calculated CO_2 mole fractions with only air–sea CO_2 flux ($[CO_2]^{OC}$, T106) are given in panel (a), and the results of the model APO simulations with both resolutions (T42 and T106) are shown in panel (b). Each value plotted for $\delta(O_2/N_2)$, CO_2 and APO was obtained as a deviation from the corresponding best-fit curve shown in Fig. 2. Grey shaded times represent the time intervals regarded as 'high APO', defined as over 10 per meg of ΔAPO, in the backward trajectory calculations (see Fig. 6). The vertical axis of APO is scaled 2 times compared to that of $\delta(O_2/N_2)$.
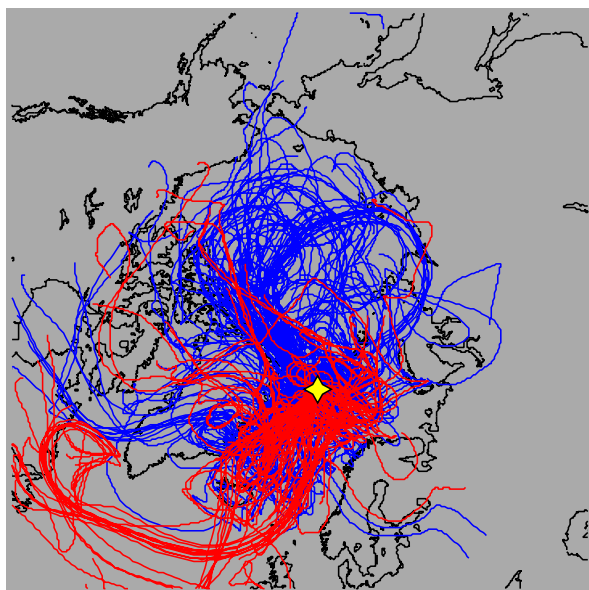

Fig. 6. Ten-day backward trajectories calculated for air parcels released from Ny-Ålesund (yellow star) every 6 h from 9 May to 29 June 2013. Red and blue lines indicate the trajectories for high and low APO, respectively.

cannot currently be achieved due to the unavailability of more detailed distributions of surface fluxes (currently $1° \times 1°$ in horizontal and monthly time intervals).

Tagged tracer experiments were performed using the ACTM with the T106 resolution, employing prescribed oceanic fluxes of O_2, N_2 and CO_2, to estimate the contributions of five different sea regions to the observed APO variations. The APO values predicted for the different regions during 9 May–29 June 2013 and the total are shown in Fig. 7a. The total APO values predicted for the five regions agree with the observed variations fairly well (Fig. 5b), although the model simulations show smaller short-term fluctuations than the observation, mainly due to prescribed oceanic O_2, N_2 and CO_2 fluxes on a monthly basis and partly due to uncertainties in the atmospheric transport of the ACTM. The contributions of the regions to the total APO, derived from the results shown in Fig. 7a, are given in Fig. 7b. The tagged tracer experiments show that the APO value stabilizes temporally when the contributions from areas far from Ny-Ålesund take precedence over those from its peripheral areas. This result is likely due to the mixing of air during its transportation over long distances. For example, the
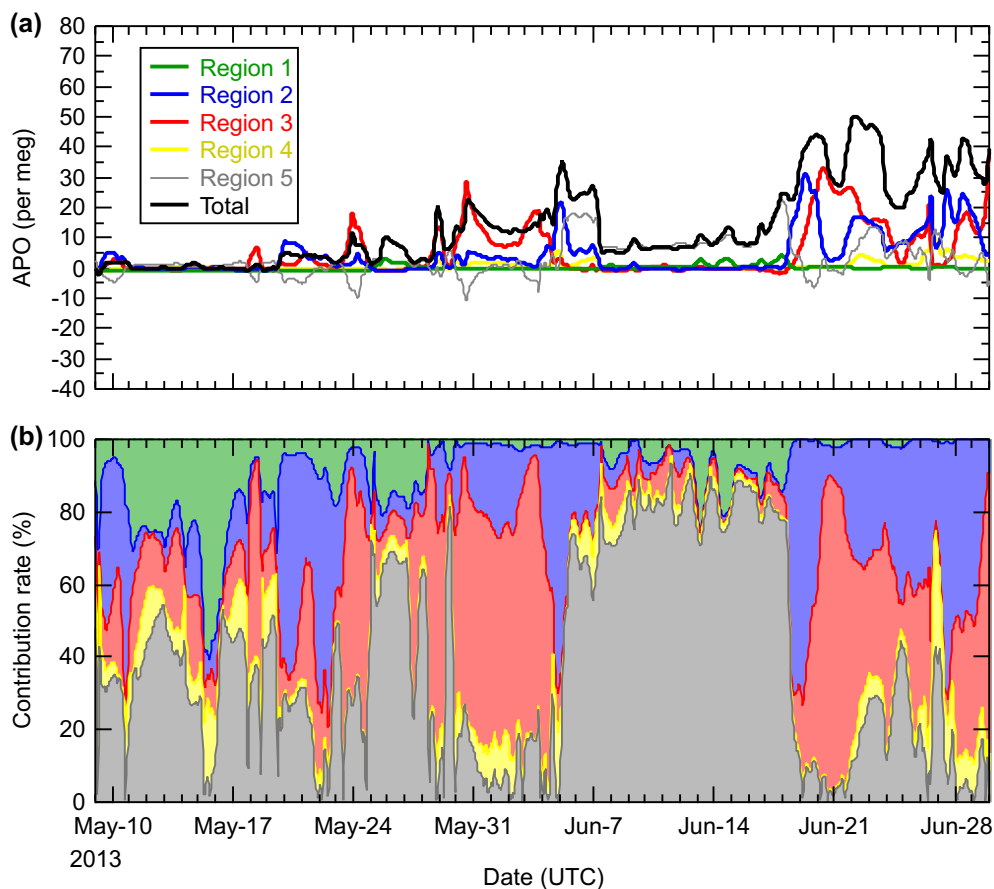
Fig. 7. (a) APO simulated using the ACTM for five tag regions and the total for the period from 9 May to 29 June 2013, and (b) contributions of the respective regions to the total.

very small APO fluctuations between 6 and 18 June 2013 are produced predominantly by air masses transported from Region 5 (the rest of the world excluding Regions 1–4), while Regions 1 and 5 show near-constant APO values between 11 and 20 May 2013. The tagged tracer experiments also indicate that Regions 2 and 3, which correspond to the Greenland Sea, the Norwegian Sea and the Barents Sea, are the main contributors to the observed short-term APO fluctuations at Ny-Ålesund in spring and early summer. This is consistent with the comparison of backward trajectories.

To examine the observed short-term APO fluctuations in more detail, we selected some characteristic events, which are indicated by green arrows in Fig. 5b. The predicted trajectories for the respective events are presented in Fig. 8a for May 2013 and Fig. 8b for June 2013. Figure 8c and d shows the distribution of monthly average marine net primary production (NPP) for May and June, as obtained from the vertically generalized production model (VGPM; Behrenfeld and Falkowski, 1997, http://www.science.oregonstate.edu/ocean.productivity/standard.product.php). By comparing the trajectories with the NPP distributions, high APO values were found to occur when air from the Norwegian Sea, the Greenland Sea or the Barents Sea

with high NPP reached the Ny-Ålesund site. Air that arrived at Ny-Ålesund after moving over the Arctic Ocean, Greenland or other low-NPP areas resulted in low or stable APO values. Oceans with high NPP emit O_2 through marine biological activity, while oceans covered with sea-ice have a significantly reduced O_2 exchange between the atmosphere and ocean. The observed short-term fluctuations in APO at Ny-Ålesund in spring and early summer would be thus likely to be caused by the O_2 emissions from high marine biological production in the seas around the Svalbard Islands. In this regard, Yamagishi et al. (2008) found similar short-term APO fluctuations in the results of continuous measurements at Cape Ochi-ishi (43°10′N, 145°30′E), Japan. By comparing observed APO variations with distributions of marine NPP, using a back trajectory analysis, they reported that such fluctuations are associated with the spring phytoplankton bloom in the Okhotsk Sea and the Western North Pacific.

3.3. *Estimates of oceanic O_2 flux and marine NCP*

Here, we estimate sea-to-air fluxes of O_2 using the observed APO fluctuations and backward trajectory analysis for spring
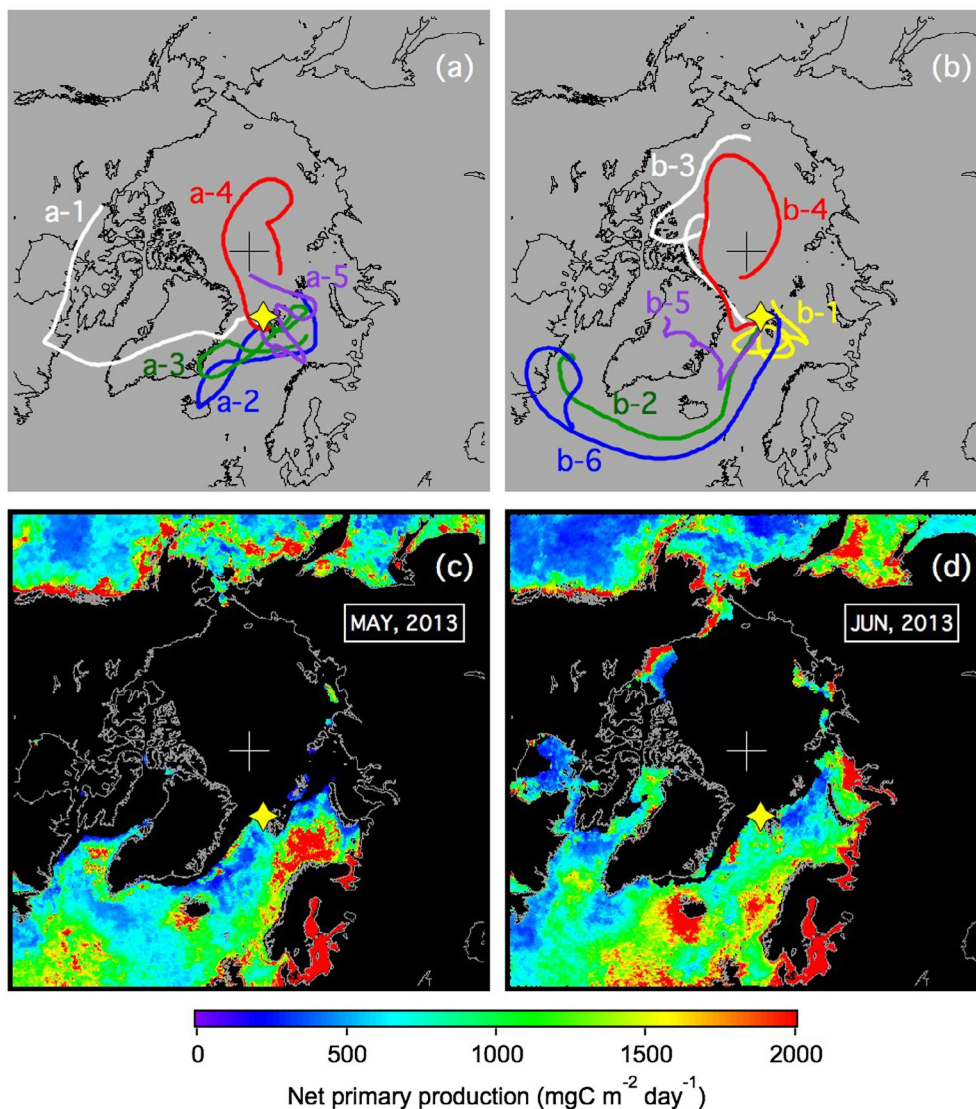
Fig. 8. Ten-day backward trajectories of air parcels released from Ny-Ålesund at selected times as indicated in Fig. 5a and b and the distributions of monthly averaged marine net primary production estimated using the Vertically Generalized Production Model (c and d) for May and June 2013. The yellow star in each panel represents the location of Ny-Ålesund.

Table 1. Summary of sea-to-air O_2 fluxes and marine NCP estimated for May and June 2013 using a well-mixed moving column model.

Event no.	Date	ΔC (per meg)	Estimated O_2 flux (μmol/m^2/day)	Estimated NCP (mgC/m^2/day)	NPP from VGPM (mgC/m^2/day)
a-2	20 May	15	1.3×10^5	1.1×10^3	~0.5×10^3
a-3	24 May	20	1.5×10^5	1.3×10^3	~2.0×10^3
a-5	30–31 May	50	4.7×10^5	4.0×10^3	~2.0×10^3
b-1	3–4 June	35	2.5×10^5	2.1×10^3	~1.5×10^3
b-2	5 June	45	5.0×10^5	4.3×10^3	~2.0×10^3
b-5	17–19 June	50	2.6×10^5	2.2×10^3	~2.0×10^3
b-6	23 June	45	2.2×10^5	1.9×10^3	~2.0×10^3

and early summer, assuming that the observed fluctuations are caused by O_2 emissions from marine biological production. As an example, we first focus on the event observed between 17

and 19 June 2013, indicated by b-5 in Fig. 5b. During this period, APO increases rapidly by about 50 per meg and then declines to close to the former level. The backward trajectory for

the time when the highest APO value was observed is shown in Fig. 8b by the purple line labelled b-5.

To estimate the sea-to-air O_2 flux, we used a well-mixed moving column model (Jacob, 1999). In this simple model, it is assumed that the vertically well-mixed air column, with a finite height, arrives at the observation site while being supplied with O_2 from the ocean. The average O_2 flux (F) into the column during transport (i.e. the sea-to-air flux) is expressed by Jacob (1999) as follows:

$$F = \frac{\Delta Ch}{t\{1 - \exp(-L/ut)\}} \quad (4)$$

where ΔC is the increase of APO in the column, h is the vertical mixing height, L is the wind fetch, u is the wind speed and t is the e-folding lifetime for the dilution of APO in the column. To calculate the flux, we used 50 per meg, 280 m, 1000 km, 4.4 m s^{-1} and 12 h for ΔC, h, L, u and t, respectively. A ΔC value of 50 per meg was taken from the observations, and t of 12 h was employed in accordance with Lueker (2004) and Thompson et al. (2007). The remaining values were determined by the following procedures. First we estimated a location where an air parcel released from Ny-Ålesund moved outside of the boundary layer. Then, the average vertical mixing height and average wind speed were calculated. The boundary layer heights and wind speeds along the air parcel trajectory leading to that location were used, while the wind fetch was calculated by integrating the distance along the trajectory. Under the given conditions, the sea-to-air O_2 flux was calculated to be 2.6×10^5 µmol m^{-2} day^{-1}. By assuming an $-O_2$:C exchange ratio of 1.4 for marine organic matter (Laws, 1991; Anderson, 1995), NCP was estimated to be 2.2×10^3 mgC m^{-2} day^{-1} from the calculated sea-to-air O_2 flux.

The same procedures as above were applied to the other events designated as a-2, a-3, a-5, b-1, b-2 and b-6 in Fig. 5. The results are summarized in Table 1, together with the relevant parameter values. The sea-to-air O_2 fluxes estimated from the events are between 1.3×10^5 and 5.0×10^5 µmol m^{-2} day^{-1}, with an average of $2.8 \pm 1.5 \times 10^5$ µmol m^{-2} day^{-1}, showing a good agreement with each other. Similarly, a good agreement is found in the calculated NCP, which range between 1.1×10^3 and 4.3×10^3 mgC m^{-2} day^{-1}, with an average value of $2.4 \pm 1.3 \times 10^3$ mgC m^{-2} day^{-1}. These values of NCP are fairly close to the NPP values of 0.5×10^3–2.0×10^3 mgC m^{-2} day^{-1} derived using the VGPM for sea areas with high biological production. The values are also consistent, within an order of magnitude, with NPP in seas where the backward trajectories predicted air parcels passed before arriving at Ny-Ålesund (Fig. 8a and b).

The sea-to-air O_2 fluxes and NCP estimated using the simple model in this study have more or less uncertainties. For example, in the case of b-5, change of 50 m in the vertical mixing height yields approximately 0.7×10^5 µmol m^{-2} day^{-1} for sea-to-air O_2 flux and 0.6×10^3 mgC m^{-2} day^{-1} for NCP. If the air–sea

CO_2 exchange is responsible for the observed CO_2 dips shown in Fig. 5a, then the APO value is also affected by the oceanic CO_2 flux. In this case, the sea-to-air O_2 flux derived from the observed APO is overestimated. However, the overestimation of the O_2 flux was calculated to be 13% at most for the case of b-5, on the assumption that all of the observed CO_2 dip is produced only by the ocean. In addition, since the observed APO fluctuations include the effect of atmospheric transport to some extent, the calculated NCP is possibly overestimated. Considering these uncertainties, it is difficult to strictly quantitatively compare NCP, derived in this study, with NPP obtained from satellite observations. However, the present results suggest that the continuous record of APO at Ny-Ålesund, especially for spring and early summer, is useful for detecting marine biological productivity signals in its peripheral seas.

4. Concluding remarks

To contribute to a better understanding of the global carbon cycle and air–sea O_2 exchange, continuous *in situ* measurements of atmospheric $\delta(O_2/N_2)$ and CO_2 mole fraction were started at a remote station Ny-Ålesund in November 2012. This instrument set-up is controlled remotely, as a first trial in the Arctic region, serviced annually by the personnel from Tohoku University and NIPR. From the measurements, a continuous record of APO was derived. The results of the first two years of measurements show a clear seasonal cycle in $\delta(O_2/N_2)$, CO_2 mole fractions and APO. We also performed numerical simulations of APO using the JAMSTEC's ACTM with prescribed oceanic O_2, N_2 and CO_2 fluxes.

Previous studies using a discrete flask sampling technique reported that the observed APO value is clearly higher than the model-simulated value in autumn, but such a difference was not found in this study for the short period of 2013–2014 (correlation coefficient = 0.99 and slope = 0.86 between the observed and simulated values). To better understand the interannual variability of the seasonal APO cycle, longer term measurements of APO and further model studies are required.

Irregular fluctuations in APO were observed, especially in spring and early summer, showing a rapid increase and decrease of up to 50 per meg on a timescale of hours to days. A comparison of the observed APO with model simulations and backward trajectories with marine NPP distributions suggests that such fluctuations are possibly caused by O_2 emissions associated with marine biological production in the Greenland Sea, the Norwegian Sea and the Barents Sea. The sea-to-air O_2 fluxes in the peripheral seas of Ny-Ålesund are estimated to be approximately $2.8 \pm 1.5 \times 10^5$ µmol m^{-2} day^{-1} by analysing selected events of irregular APO fluctuations, using a well-mixed moving column model. The average marine NCP calculated from these sea-to-air O_2 fluxes is about $2.4 \pm 1.3 \times 10^3$ mgC m^{-2} day^{-1}, comparable with NPP estimated using the VGPM for seas with high biological production. These results indicate that our measurements

of APO at Ny-Ålesund are useful for examining marine biological productivity in the surrounding seas.

It was recently reported that annual NPP in the Arctic Ocean increased by about 20% between 1998 and 2009, due to an increase in the extent of open water by the ongoing decrease of sea ice (Arigo and van Dijken, 2011). It is likely that the increase in NPP will enhance oceanic CO_2 uptake, changing the carbon cycle in the Arctic Ocean. However, it is also recognized that there is a large CO_2 variability in the surface layer of the Arctic Ocean, meaning it is not always a significant CO_2 sink (Cai et al., 2010). Our continuous observations of atmospheric $\delta(O_2/N_2)$ and CO_2 mole fraction at Ny-Ålesund can play an important role in detecting possible changes in the carbon cycle in the Arctic region during the near future.

Acknowledgements

Disclosure statement

No potential conflict of interest was reported by the authors.

Funding

References

Anderson, L. 1995. On the hydrogen and oxygen content of marine phytoplankton. *Deep Sea Res., Part I* **42**, 1675–1680. DOI:10.1016/0967-0637(95)00072-E.

Arigo, K. R. and van Dijken, G. L. 2011. Secular trends in Arctic Ocean net primary production. *J. Geophys. Res.* **116**, C09011. DOI:10.1029/2011JC007151.

Battle, M., Fletcher, S. M., Bender, M. L. and Keeling, R. F. 2006. Atmospheric potential oxygen: new observations and their implications for some atmospheric and oceanic models. *Global Biogeochem. Cycles* **20**, GB1010. DOI:10.1029/2005GB002534.

Behrenfeld, M. J. and Falkowski, P. G. 1997. Photosynthetic rates derived from satellite-based chlorophyll concentration. *Limnol. Oceanogr.* **42**, 1–20.

Bender, M. L., Ho, D. T., Hendricks, M. B., Mika, R., Battle, M. O. and co-authors. 2005. Atmospheric O2/N2 changes, 1993–2002: implications for the partitioning of fossil fuel CO2 sequestration. *Global Biogeochem. Cycles* **19**, GB4017. DOI:10.1029/2004GB002410.

Blaine, T. W. 2005. *Continuous Measurements of the Atmospheric Ar N_2 Ratio as a Tracer of Air–Sea Heat Flux: Models, Methods, and Data*, PhD thesis University of California, San Diego, CA.

Cai, W.-J., Chen, L., Chen, B., Gao, Z., Lee, S. H. and co-authors. 2010. Decrease in the CO_2 uptake capacity in an ice-free Arctic Ocean basin. *Science* **329**, 556–559.

Engardt, M., Holmén, K. and Heintzenberg, J. 1996. Short-term variations in atmospheric CO_2 at Ny-Ålesund, Spitsbergen, during spring and summer. *Tellus B* **48**, 33–43.

Garcia, H. and Keeling, R. 2001. On the global oxygen anomaly and air-sea flux. *J. Geophys. Res.* **106**, 31155–31166.

Goto, D., Morimoto, S., Aoki, S. and Nakazawa, T. 2013a. High precision continuous measurement system for the atmospheric O_2/N_2 ratio at Ny-Ålesund, Svalbard and preliminary observational results. *Nankyoku Shiryo (Antarct. Rec.)* **57**, 17–27.

Goto, D., Morimoto, S., Ishidoya, S., Ogi, A., Aoki, S. and co-authors. 2013b. Development of a high precision continuous measurement system for the atmospheric O_2/N_2 ratio and its application at Aobayama, Sendai. *Japan. J. Meteorol. Soc. Japan* **91**(2), 179–192.

Ishidoya, S., Aoki, S., Goto, D., Nakazawa, T., Taguchi, S. and co-authors. 2012a. Time and space variations of the O_2/N_2 ratio in the troposphere over Japan and estimation of global CO_2 budget. *Tellus B* **64**, 18964. DOI:10.3402/tellusb.v64i0.18964.

Ishidoya, S., Aoki, S. and Nakazawa, T. 2003. High precision measurements of the atmospheric O_2/N_2 ratio on a mass spectrometer. *J. Meteorol. Soc. Japan* **81**, 127–140.

Ishidoya, S., Morimoto, S., Aoki, S., Taguchi, S., Goto, D. and co-authors. 2012b. Oceanic and terrestrial biospheric CO_2 uptake estimated from atmospheric potential oxygen observed at Ny-Ålesund, Svalbard, and Syowa, Antarctica. *Tellus B* **64**, 18924. DOI:10.3402/tellusb.v64i0.18924.

Ishidoya, S., Murayama, S., Takamura, C., Kondo, H., Saigusa, N. and co-authors. 2013. O_2:CO_2 exchange ratios observed in a cool temperate deciduous forest ecosystem of central Japan. *Tellus B* **65**, 21120. DOI:10.3402/tellusb.v65i0.21120.

Ishidoya, S., Uchida, H., Sasano, D., Kosugi, N., Taguchi, S. and co-authors. 2016. Ship-based observations of atmospheric potential oxygen and regional air sea O_2 flux in the northern North Pacific and the Arctic Ocean. *Tellus B* **68**, 29972. DOI:10.3402/tellusb.v68.29972.

Jacob, D. 1999. *Introduction to Atmospheric Chemistry*. Princeton University Press, Princeton, NJ, 266pp.

Keeling, R. F., Najjar, R. P. and Bender, M. L. 1993. What atmospheric oxygen measurements can tell us about the global carbon cycle. *Global Biogeochem. Cycles* **7**, 37–67.

Keeling, R. F. and Manning, A. C. 2014. Studies of recent changes in atmospheric O_2 content. In: *Treatise on Geochemistry* (eds. H. Holland and K. Turekian). Vol. 5.15, Elsevier, Amsterdam, pp. 385–404.

Keeling, R. F. and Shertz, S. R. 1992. Seasonal and interannual variations in atmospheric oxygen and implications for the global carbon cycle. *Nature* **358**, 723–727.

Laws, E. A. 1991. Photosynthetic quotients, new production and net community production in the open ocean. *Deep Sea Res., Part A* **38**, 143–167.

Lueker, T. J. 2004. Coastal upwelling fluxes of O_2, N_2O, and CO_2 assessed from continuous atmospheric observations at Trinidad, California. *Biogeosciences* **1**, 101–111.

Lueker, T. J., Walker, S. J., Vollmer, M. K., Keeling, R. F., Nevison, C. D. and co-authors. 2003. Coastal upwelling air-sea fluxes revealed in atmospheric observations of O_2/N_2, CO_2 and N_2O. *Geophys. Res. Lett.* **30**, 1292. DOI:10.1029/2002GL016615.

Manning, A. C. and Keeling, R. F. 2006. Global oceanic and terrestrial biospheric carbon sinks from the Scripps atmospheric oxygen flask sampling network. *Tellus B* **58**, 95–116.

Maturilli, M., Herber, A. and König-Langlo, G. 2013. Climatology and time series of surface meteorology in Ny-Ålesund, Svalbard. *Earth Syst. Sci. Data* **5**, 155–163.

Nakaoka, S., Aoki, S., Nakazawa, T., Hashida, G., Morimoto, S. and co-authors. 2006. Temporal and spatial variations of oceanic pCO_2 and air–sea CO_2 flux in the Greenland Sea and the Barents Sea. *Tellus* **58B**, 148–161.

Nakazawa, T., Ishizawa, M., Higuchi, K. and Trivett, N. B. A. 1997. Two curve fitting methods applied to co2 flask data. *Environmetrics* **8**, 197–218.

Nevison, C. D., Mahowald, N. M., Doney, S. C., Lima, I. D. and Cassar, N. 2008. Impact of variable air-sea O_2 and CO_2 fluxes on atmospheric potential oxygen (APO) and land-ocean carbon sink partitioning. *Biogeosciences* **5**, 875–889.

Onogi, K., Tsutsui, J., Koide, H., Sakamoto, M., Kobayashi, S. and co-authors. 2007. The JRA-25 reanalysis. *J. Meteorol. Soc. Japan.* **85**, 369–432.

Patra, P. K., Krol, M. C., Montzka, S. A., Arnold, T., Atlas, E. L. and co-authors. 2014. Observational evidence for interhemispheric hydroxyl-radical parity. *Nature* **513**, 219–223.

Patra, P. K., Takigawa, M., Dutton, G. S., Uhse, K., Ishijima, K. and co-authors. 2009. Transport mechanisms for synoptic, seasonal and interannual SF_6 variations and 'age' of air in troposphere. *Atmos. Chem. Phys.* **9**, 1209–1225.

Press, W. H., Tuekolsky, S. A., Vetterling, W. T. and Flannery, B. P. 2007. *Numerical Recipes: The Art of Scientific Computing*, 3rd ed. Cambridge University Press, New York, NY.

Shulenberger, E. and Reid, J. L. 1981. The Pacific shallow oxygen maximum, deep chlorophyll maximum, and primary productivity, reconsidered. *Deep Sea Res.* **28**, 901–919.

Stephens, B. B., Keeling, R. F., Heimann, M., Six, K., Murnane, R. and co-authors. 1998. Testing global ocean carbon cycle models using measurements of atmospheric O_2 and CO_2 concentration. *Global Biogeochem. Cycles* **12**, 213–230.

Takahashi, T., Sutherland, S. C., Wanninkhof, R., Sweeney, C., Feely, R. A. and co-authors. 2009. Climatological mean and decadal change in surface ocean pCO_2, and net sea–air CO_2 flux over the global oceans. *Deep-Sea Res. II* **56**, 554–577.

Tohjima, Y., Minejima, C., Mukai, H., Machida, T., Yamagishi, H. and co-authors. 2012. Analysis of seasonality and annual mean distribution of the atmospheric potential oxygen (APO) in the Pacific region. *Global Biogeochem. Cycles* **26**, GB4008. DOI:10.1029/2011GB004110.

Tohjima, Y., Mukai, H., Machida, T., Nojiri, Y. and Gloor, M. 2005. First measurements of the latitudinal atmospheric O_2 and CO_2 distributions across the western Pacific. *Geophys. Res. Lett.* **32**, L17805.

Tohjima, Y., Mukai, H., Nojiri, Y., Yamagishi, H. and Machida, T. 2008. Atmospheric O_2/N_2 measurements at two Japanese sites: estimation of global oceanic and land biotic carbon sinks and analysis of the variations in atmospheric potential oxygen (APO). *Tellus B* **60**, 213–225.

Tohjima, Y., Terao, Y., Mukai, H., MacHida, T., Nojiri, Y. and co-authors. 2015. ENSO-related variability in latitudinal distribution of annual mean atmospheric potential oxygen (APO) in the equatorial Western Pacific. *Tellus B* **67**, 25869. DOI:10.3402/tellusb.v67.25869.

Thompson, R. L., Manning, A. C., Lowe, D. C. and Weatherburn, D. C. 2007. A ship-based methodology for high precision atmospheric oxygen measurements and its application in the Southern Ocean region. *Tellus B* **59**, 643–653. DOI:10.1111/j.16000889.2007.00292.x.

van der Laan-Luijkx, I. T., Neubert, R. E. M., van der Laan, S. and Meijer, H. A. J. 2010. Continuous measurements of atmospheric oxygen and carbon dioxide on a North Sea gas platform. *Atmos. Meas. Tech.* **3**, 113–125.

Yamagishi, H., Tohjima, Y., Mukai, H. and Sasaoka, K. 2008. Detection of regional scale sea-to-air oxygen emission related to spring bloom near Japan by using in situ measurements of the atmospheric oxygen/nitrogen ratio. *Atmos. Chem. Phys.* **8**, 3325–3335.

Zeng, J., Katsumoto, M., Ide, R., Inagaki, M., Mukai, H. and Fujinuma, Y. 2003. Development of meteorological data explorer for Windows. In: *Data Analysis and Graphic Display System for Atmospheric Research using PC, CGER-M014-2003* (ed. Y. Fujinuma). Center for Global Environmental Research/NIES, Tsukuba, pp. 19–73.